Letter

# Efficient verification of entangled continuous-variable quantum states with local measurements

Ye-Chao Liu ⬤, Jiangwei Shang ⬤,[*] and Xiangdong Zhang[†]

*Key Laboratory of Advanced Optoelectronic Quantum Architecture and Measurement of Ministry of Education,*
*School of Physics, Beijing Institute of Technology, Beijing 100081, China*

Continuous-variable quantum states are of particular importance in various quantum information processing tasks including quantum communication and quantum sensing. However, a bottleneck has emerged with the fast increasing in size of the quantum systems which severely hinders their efficient characterization. In this work, we establish a systematic framework for verifying entangled continuous-variable quantum states by employing local measurements only. Our protocol is able to achieve the unconditionally high verification efficiency which is quadratically better than quantum tomography as well as other nontomographic methods. Specifically, we demonstrate the power of our protocol by showing the efficient verification of entangled two-mode and multimode coherent states with local measurements.

*Introduction.* Continuous-variable (CV) quantum systems have demonstrated their unique role in various quantum information processing applications [1,2]. Because of the quantum description of the electromagnetic field, they are particularly relevant for quantum communication and quantum-enhanced techniques including sensing, detecting, and imaging. Also, the atomic and solid state CV systems have the potential for quantum computing. The actual realization of all these applications must depend on the efficient and reliable characterization of the quantum states in the first place. The standard method of quantum state tomography (QST) [3–9] is able to obtain all the information about the quantum states based on the Wigner function or the density matrix with a certain precision. As powerful as it is, however, QST consumes too much resource, which is the reason why other nontomographic methods have been developed [10–15].

Recently, a new characterization method called quantum state verification (QSV) has been systematically investigated in discrete-variable (DV) quantum systems [16,17]. The task of QSV is to verify that a given quantum device does indeed produce a particular target state that we expect. The core advantage of QSV lies in its asymptotically quadratic improvement of the verification efficiency as compared to other methods. By the specific design, QSV can efficiently or even optimally verify many different kinds of multipartite quantum states with local measurements only [18–34], and the methodology can also be extended to verify quantum processes [35–37]. Considering CV quantum systems, however,

even if the truncation method can reduce the dimension of the CV states from infinite to finite, the limited choice of measurements makes that the generalization of QSV to CV systems is, in general, hard.

To characterize CV quantum states, intensity measurements based on quadratures are usually employed in quantum tomography and other nontomographic methods. The intensity measurements are especially suitable for Gaussian states, as they can be fully characterized by expectation values of the quadratic operators. However, they are, in principle, inappropriate for the task of quantum verification since postprocessing of the experimental data is needed for estimating the quadratures. Except for some special quantum states defined by quadratures directly like the CV cluster states [38], of which the verification protocol can be generalized from the discrete scenario [15]. Hence, we consider the energy-based photon counting measurements, the realization of which relies on the single-photon detector (SPD) and the more general photon number resolution detector (PNRD) [39–43]. These measurements can realize projections on the Fock bases, as well as projections on the coherent states with the help of displacement operations. Thus, postprocessing of the data can be avoided by using these "deterministic" measurements. Note, in particular, different from the recent work by Wu *et al.* [44] on the verification of CV quantum states which demands a necessary preprocessing step for the samples to satisfy the condition of independent and identical distribution (i.i.d.), the intrinsic nature of QSV is in general exempt from this requirement. Hence, in the non-i.i.d. scenarios, QSV stands out as a much more efficient method in terms of the resource cost.

In this work, we propose a systematic framework for verifying entangled CV quantum states with the help of local measurements only. Our protocol is able to achieve the unconditionally high verification efficiency with the resource overhead given by $N \propto O(\epsilon^{-1} \ln \delta^{-1})$ within infidelity $\epsilon$ and confidence level $1 - \delta$, which is quadratically better

*[*]jiangwei.shang@bit.edu.cn
*[†]zhangxd@bit.edu.cn

than quantum tomography as well as other nontomographic methods [10–15]. For demonstration, we show the efficient verification of entangled two-mode as well as multimode coherent states with local measurements. These states are crucial in various quantum information processing tasks including quantum teleportation [45,46], quantum computation [47–50], and quantum metrology [51–53]. Moreover, a general optimization strategy is given in order to achieve the optimal efficiency for the specific scenarios under consideration.

*General framework.* The task of quantum state verification is to determine whether the states $\sigma_1, \sigma_2, \ldots$ output from a device, all of which are supposed to be the target state $|\psi\rangle$ (DV or CV), are cases either $\sigma_i = |\psi\rangle\langle\psi|$ for all $i$, or $\langle\psi|\sigma_i|\psi\rangle \leqslant 1 - \epsilon$ for all $i$. Then, a verification protocol $\Omega$ can be generally constructed by several dichotomic-outcome projective measurement settings $\{\Omega_l, \mathbb{1} - \Omega_l\}$, such that

$$\Omega = \sum_l \mu_l \Omega_l, \tag{1}$$

where $\{\mu_l\}$ is a probability distribution. With the requirement that the target state should always pass all the measurements, i.e., $\langle\psi|\Omega_l|\psi\rangle = 1$, errors of the verification protocol occur only when the noisy states $\sigma$ pass the protocol with the maximal probability [17,25]

$$\max_{\langle\psi|\sigma|\psi\rangle \leqslant 1-\epsilon} \operatorname{tr}(\Omega\sigma) = 1 - [1 - \lambda_2(\Omega)]\epsilon = 1 - \nu\epsilon, \tag{2}$$

where $\lambda_2(\Omega)$ is the second-largest eigenvalue of $\Omega$, and $\nu := 1 - \lambda_2(\Omega)$ denotes the spectral gap from the maximal eigenvalue. Then, after $N$ measurements, the maximal worst-case probability that the verifier fails to detect the "bad" case is given by $(1 - \nu\epsilon)^N$. Hence, to achieve a confidence level $1 - \delta$, the number of copies of the states required is

$$N \geqslant \frac{1}{\ln[(1-\nu\epsilon)^{-1}]} \ln\delta^{-1} \approx \frac{1}{\nu}\epsilon^{-1}\ln\delta^{-1}. \tag{3}$$

In practice, searching for the optimal verification protocol is a demanding task, if not impossible at all. For CV quantum states, in particular, the intrinsic nature of their infinite dimensional Hilbert space makes the spectral decomposition for $\Omega$ even more challenging. To render the task, we may restrict the type of noisy states to be in some specific form. Here, we focus on the noisy states such that $\langle\psi|\sigma_i|\psi\rangle = 1 - \epsilon$ for all $i$, which is allowable since other states with $\langle\psi|\sigma_i|\psi\rangle < 1 - \epsilon$ would not make the verification worse [17], thus the original task is retained. By choosing a set of bases $\mathcal{S}$ constructed from the target state $|\psi\rangle$ and all of the mutually orthonormal states $\{|\psi_{i,j}^\perp\rangle\}$ that form the subspace orthogonal to $|\psi\rangle$, we can write the noisy states as

$$\sigma_i = (1 - \epsilon)|\psi\rangle\langle\psi| + \sum_j \epsilon_{i,j}|\psi_{i,j}^\perp\rangle\langle\psi_{i,j}^\perp| + \text{N.D.}, \tag{4}$$

where $\sum_j \epsilon_{i,j} = \epsilon$ and N.D. represents the nondiagonal terms in $\mathcal{S}$, i.e., $|\phi'\rangle\langle\phi|$ for all $|\phi'\rangle \neq |\phi\rangle \in \mathcal{S}$. Thus, the optimization for the spectral gap can be reduced to

$$\nu_{\text{opt}} := \max_\Omega \min_i \sum_l \mu_l k_{l,i}, \tag{5}$$

where $k_{l,i} := 1 - \sum_j \frac{\epsilon_{i,j}}{\epsilon}\langle\psi_{i,j}^\perp|\Omega_l|\psi_{i,j}^\perp\rangle \in [0, 1]$ (see Supplemental Material Appendix A [54] for the detailed derivation).

Note that the above framework including the optimization method works for both the CV and DV scenarios.

*One-mode coherent state superpositions.* The one-mode coherent states are defined as

$$|\alpha\rangle = e^{-|\alpha|^2/2} \sum_{n=0}^\infty \frac{\alpha^n}{\sqrt{n!}}|n\rangle, \quad \text{with } \alpha \in \mathbb{C}, \tag{6}$$

where $|n\rangle$ denotes the Fock states (or number states), which form a complete set of bases in the Hilbert space. The verification of $|\alpha\rangle$ can be easily done by invoking the projective measurement $|\alpha\rangle\langle\alpha|$, which is achievable via a Kennedy receiver [55,56], i.e., a SPD combined with the displacement $D(-\alpha)$ in front,

$$|\alpha\rangle\langle\alpha| \equiv D^\dagger(-\alpha)|0\rangle\langle0|D(-\alpha). \tag{7}$$

Then, we consider the superposition of one-mode coherent states, usually referred to as the coherent state superpositions (CSSs) [57,58]. Typical examples of CSSs are the even and odd coherent cat states [59],

$$|+_\alpha\rangle = \frac{|\alpha\rangle + |-\alpha\rangle}{\sqrt{C_+^{(\alpha)}}}, \quad |-_\alpha\rangle = \frac{|\alpha\rangle - |-\alpha\rangle}{\sqrt{C_-^{(\alpha)}}}, \tag{8}$$

with the normalization $C_\pm^{(\alpha)} = 2(1 \pm e^{-2|\alpha|^2})$. They are useful in various quantum information processing tasks including quantum teleportation [45], quantum computation [49,50], and quantum metrology [60]. These two cat states can be discriminated using the parity measurement [61,62]

$$\pi = \sum_n |2n\rangle\langle2n| - \sum_n |2n+1\rangle\langle2n+1|, \tag{9}$$

such that

$$\pi^+|+_\alpha\rangle = |+_\alpha\rangle, \quad \pi^-|-_\alpha\rangle = |-_\alpha\rangle, \tag{10}$$

which can be realized by PNRDs. The superscripts $\pm$ indicate the projectors onto the eigenspace with the corresponding eigenvalues $\pm1$. Note, however, that the parity measurement solely is not sufficient to verify the even or odd coherent cat states, as for instance, $|+_\alpha\rangle$ and $|+_\beta\rangle$ with $\alpha \neq \pm\beta$ have the same behavior under the parity measurement.

Upon this point, we have revealed a significant difference between CV and DV quantum states regarding their verification, namely, the CSSs including the symmetric cat states, cannot be verified straightforwardly. The reason is due to the intrinsic nature of the infinite dimension of CV systems which results in the fact that realization of a deterministic arbitrary local operation in CV is still an open problem. Nevertheless, some of the entanglement operations in CV are easier to implement instead. For instance, in optical systems, consider the beam splitter (BS) with the form

$$B(\theta) = \exp[i\theta(\hat{a}_1^\dagger \hat{a}_2 + \hat{a}_1 \hat{a}_2^\dagger)], \tag{11}$$

where $\hat{a}_{1(2)}^\dagger, \hat{a}_{1(2)}$ are the creation and annihilation operators for the first (second) mode, respectively. The parameter $\theta \in (0, \frac{\pi}{2})$ determines the transmissivity of the BS, i.e., $\cos^2\theta \in (0, 1)$. Then, by coupling to an ancilla vacuum mode $|0\rangle$, we can convert, for example, the even coherent cat state

to

$$B(\theta)|+_\alpha\rangle|0\rangle = \frac{1}{\sqrt{C_+^{(\alpha)}}}(|\alpha\cos\theta\rangle|i\alpha\sin\theta\rangle$$
$$+ |-\alpha\cos\theta\rangle|-i\alpha\sin\theta\rangle). \quad (12)$$

This is the entangled coherent state, which we show how to verify in the next section.

*Two-mode entangled coherent states.* The entangled coherent states (ECSs) usually refer to the superposition of two-mode coherent states with the form $|\alpha\rangle|0\rangle + |0\rangle|\alpha\rangle$ (unnormalized) specifically [63,64]. Here, we consider a more general form such that

$$\left|\psi_{\alpha,\beta}^{\mathrm{ECS}}\right\rangle = \frac{1}{\sqrt{C_{\alpha,\beta}}}(|\alpha\rangle|0\rangle + |0\rangle|\beta\rangle), \quad (13)$$

where the normalization is $C_{\alpha,\beta} = 2[1 + e^{-(|\alpha|^2+|\beta|^2)/2}]$. Note that the transformed even coherent cat state in Eq. (12) is a special case of $|\psi_{\alpha,\beta}^{\mathrm{ECS}}\rangle$ under proper local displacement operations. Furthermore, a class of more general entangled states with the form (unnormalized)

$$|\tilde\psi^{\mathrm{ECS}}\rangle := |\alpha_1\rangle|\alpha_2\rangle + |\beta_1\rangle|\beta_2\rangle \quad (14)$$

is locally equivalent to $|\psi_{\alpha,\beta}^{\mathrm{ECS}}\rangle$ when $\alpha_{1,2}, \beta_{1,2} \in \mathbb{R}$ [65,66] (see Supplemental Material Appendix B [54] for all the derivations).

Although similar in form as the Bell states in the DV scenario, verification of the two-mode $|\psi_{\alpha,\beta}^{\mathrm{ECS}}\rangle$ cannot use the analytical technique as in Ref. [21] or the numerical approach as in Ref. [20]. The infinite dimensional Hilbert space of the CV systems severely restricts the type of measurements that can be realizable. Hence, we start by fully exploring their physical properties.

Measurements of the SPDs can be described by $\{\tau^+ = |0\rangle\langle 0|, \tau^- = \mathbb{1} - |0\rangle\langle 0|\}$, using which one finds the relation $(\tau^- \otimes \tau^-)|\psi_{\alpha,\beta}^{\mathrm{ECS}}\rangle = 0$. Thus, to verify $|\psi_{\alpha,\beta}^{\mathrm{ECS}}\rangle$, the first measurement setting we can employ is

$$\Omega_1^{\mathrm{ECS}} = \mathbb{1} - \tau^- \otimes \tau^- = \mathbb{1} - \sum_{n,m=1}^\infty (|n\rangle\langle n| \otimes |m\rangle\langle m|), \quad (15)$$

which satisfies $\Omega_1^{\mathrm{ECS}}|\psi_{\alpha,\beta}^{\mathrm{ECS}}\rangle = |\psi_{\alpha,\beta}^{\mathrm{ECS}}\rangle$. Physically speaking, this setting implies that the target state must have at least one mode that has no photon. However, the possibility that no photons emerge from both modes together cannot be ruled out since $\langle\psi_{\alpha,\beta}^{\mathrm{ECS}}|(\tau^+ \otimes \tau^+)|\psi_{\alpha,\beta}^{\mathrm{ECS}}\rangle \neq 0$, which is rather different from the property of the DV entangled states, like the Bell states.

Next, we define the displacement operation $\mathbb{D}(-\alpha, -\beta) := D(-\alpha) \otimes D(-\beta)$ acting on the two modes, which transforms the target state $|\psi_{\alpha,\beta}^{\mathrm{ECS}}\rangle$ to another ECS state $|\psi_{-\alpha,-\beta}^{\mathrm{ECS}}\rangle$. With this, we have the following measurement setting:

$$\Omega_2^{\mathrm{ECS}} = \mathbb{D}^\dagger(-\alpha, -\beta)(\mathbb{1} - \tau^- \otimes \tau^-)\mathbb{D}(-\alpha, -\beta), \quad (16)$$

which is in fact a generalized Kennedy receiver for two-mode states.
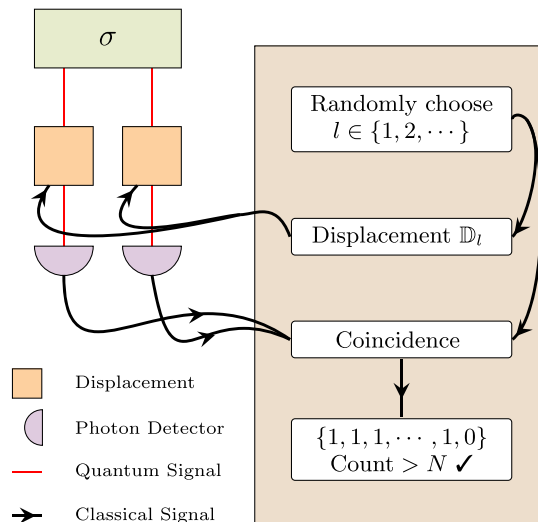


FIG. 1. General framework for the verification of two-mode entangled coherent states $|\psi_{\alpha,\beta}^{\mathrm{ECS}}\rangle$ as in Eq. (13). By randomly choosing the displacement operation $\mathbb{D}_l$, the outcomes with 1 or 0 of the coincidences of the two detectors are counted. The outcome 1 represents the "pass" instance and 0 for "fail." With the number of successive "pass" instances larger than $N$, $|\psi_{\alpha,\beta}^{\mathrm{ECS}}\rangle$ is verified.

The third measurement setting

$$\Omega_3^{\mathrm{ECS}} = \mathbb{D}^\dagger\left(-\frac{\alpha}{2}, -\frac{\beta}{2}\right)(\pi \otimes \pi)^+ \mathbb{D}\left(-\frac{\alpha}{2}, -\frac{\beta}{2}\right) \quad (17)$$

comes from the fact that ECSs have the parity symmetry under proper displacement, i.e.,

$$\mathbb{D}\left(-\frac{\alpha}{2}, -\frac{\beta}{2}\right)\left|\psi_{\alpha,\beta}^{\mathrm{ECS}}\right\rangle = \frac{C_+|+_{\alpha/2}\rangle|+_{\beta/2}\rangle - C_-|-_{\alpha/2}\rangle|-_{\beta/2}\rangle}{2\sqrt{C_{\alpha,\beta}}},$$
$$(18)$$

where $C_\pm = \sqrt{C_\pm^{(\alpha/2)}C_\pm^{(\beta/2)}}$.

Briefly speaking, the first two measurement settings $\Omega_1^{\mathrm{ECS}}$ and $\Omega_2^{\mathrm{ECS}}$ check the existence of the vacuum mode and the coherent mode, respectively. Together they ensure the superposition of the two states $|\alpha\rangle|0\rangle$ and $|0\rangle|\beta\rangle$. With the third setting $\Omega_3^{\mathrm{ECS}}$ confirming the balanced superposition, the ECSs can be verified. Hence, these three measurement settings are sufficient to verify $|\psi_{\alpha,\beta}^{\mathrm{ECS}}\rangle$; see the following theorem with its proof postponed to Supplemental Material Appendix C [54].

*Theorem 1.* The two-mode entangled coherent states $|\psi_{\alpha,\beta}^{\mathrm{ECS}}\rangle$ can be verified efficiently by the protocol

$$\Omega^{\mathrm{ECS}} = \sum_{l=1}^3 \mu_l \Omega_l^{\mathrm{ECS}}, \quad (19)$$

where the probability distribution $\{\mu_l\}$ is arbitrary. An optimal efficiency can be obtained by optimizing $\{\mu_l\}$ under specific scenarios as constrained by Eq. (5).

In Fig. 1, we show the general framework of the protocol. The target states to be verified are input into two separate channels, followed by the displacement operation $\mathbb{D}_l$, and finally measured by photon detectors. The displacement $\mathbb{D}_l$ has three different cases $\{\mathbb{D}_1 = \mathbb{1}\otimes\mathbb{1}, \mathbb{D}_2 = D(-\alpha)\otimes D(-\beta), \mathbb{D}_3 = D(-\frac{\alpha}{2}) \otimes D(-\frac{\beta}{2})\}$, which are applied on each mode

locally. PNRDs are required for the third setting $\Omega_3^{\text{ECS}}$, while the first two settings only need SPDs. The three measurement settings are randomly chosen in accordance with the probability distribution $\{\mu_l\}$. Then, the numbers of coincidences of the two detectors are counted with outcome 1 representing a "pass" instance and 0 for "fail." If the number of successive "pass" instances is larger than $N$, we confirm that the state is $|\psi_{\alpha,\beta}^{\text{ECS}}\rangle$ with certain confidence. As mentioned by Theorem 1, the sample complexity $N$ is determined by the optimal verification efficiency $1/\nu_{\text{opt}}$ which can be obtained by optimizing the probability distribution $\{\mu_l\}$ under specific scenarios as constrained by Eq. (5). Note, furthermore, if changing the balanced superposition of the two terms in ECS from $+$ to $-$, to which the transformed odd coherent cat state is locally equivalent, all the experimental settings remain the same except for $\Omega_3^{\text{ECS}}$, which differs by a sign (see Supplemental Material Appendix D [54] for more detailed discussions).

Before proceeding to give a concrete example, we have a quick remark regarding the PNRDs. In practice, finite resolution of the PNRDs for the parity measurements always leads to a systematic error. We can circumvent this problem by directly dismissing the results when PNRDs are saturated. For instance, consider the PNRD(3) with four outcomes $\{0, 1, 2, 3+\}$, such that one can keep the outcomes $\{0, 1, 2\}$ only by discarding the rest. Some efficiency will be lost during this process, and the probability to get the useful results with PNRD($r$) for a one-mode CV state $|\psi\rangle$ is given by

$$p(r) = \sum_{i=0}^{r-1} |\langle i|\psi\rangle|^2. \tag{20}$$

However, we emphasize that when $\alpha$ is small, the loss is negligible. For example, considering the one-mode even coherent cat state $|+_{\alpha}\rangle$ with $\alpha = 1$, the efficiency is about 97.2% by using PNRD(3). As for PNRD(20), which is the highest resolution currently achievable in the laboratory [39], the loss is around $10^{-16}$, which can be safely ignored.

Following the above discussion, here we demonstrate the high efficiency of our protocol by considering the verification of $|\psi_{\alpha,\alpha}^{\text{ECS}}\rangle$ with PNRD(5). The most significant decoherent noise for verifying ECSs comes from the photon loss from channels and the construction error from two-mode displacements. Hence, as a demonstration, we assume that the input noisy states $\sigma_i = |\phi_i\rangle\langle\phi_i|$ take the following forms, i.e.,

$$|\phi_e(\eta)\rangle := |\alpha - \kappa + \Delta\rangle|\kappa\rangle + |\kappa + \Delta\rangle|\alpha - \kappa\rangle, \tag{21}$$
$$|\phi_s(\eta)\rangle := |\alpha - \kappa + \Delta\rangle|\kappa + \Delta\rangle + |\kappa + \Delta\rangle|\alpha - \kappa + \Delta\rangle,$$

where the perturbation $\kappa = (1 - \sqrt{\eta})\alpha/2$ is caused by photon loss with $\eta$ denoting the fraction of photons that survives the noisy channel [45], and the small value $\Delta$ represents the displacement error. These two types of noisy states thus correspond to the extreme one-mode error and the symmetric two-mode error, respectively [67]. Then, the optimization in Eq. (5) shows that the resource requirement for verifying $|\psi_{\alpha,\alpha}^{\text{ECS}}\rangle$ is $N \approx 2.60(4)\epsilon^{-1}\ln\delta^{-1}$ with the optimized probability $\{\mu_l\} = \{0.49(7), 0.40(2), 0.10(1)\}$. As a comparison, for the tomographic detection of an ECS with a 99.99% fidelity using PNRDs, the experiment in Ref. [68] used more than $10^{10}$ measurements. Our protocol, instead, is much more

efficient which requires $\sim 10^5$ measurements to reach the confidence level of 99%. Note that this optimization procedure can be generalized to deal with various types of noises (see Supplemental Material Appendix E [54] for more detailed discussions).

*Multimode entangled coherent states.* Here we consider a class of multimode entangled coherent states with the form

$$|\psi^{\text{GHZ-}m}\rangle = \frac{1}{\sqrt{C}}\left(\bigotimes_{i=1}^{m}|\alpha_i\rangle + |0\rangle^{\otimes m}\right), \tag{22}$$

where the normalization is $C = 2[1 + e^{-\sum_i |\alpha_i|^2/2}]$. Depending on the number of modes, we refer to them as the $m$-mode GHZ-like coherent states, which are generalizations of the states in Ref. [69]. Note that, for $m = 2$, states $|\psi_{\alpha,\beta}^{\text{ECS}}\rangle$ and $|\psi^{\text{GHZ-2}}\rangle$ are locally equivalent. In fact, a class of generalized GHZ-like states

$$|\tilde{\psi}^{\text{GHZ-}m}\rangle := \bigotimes_{i=1}^{m}|\alpha_i\rangle + \bigotimes_{i=1}^{m}|\beta_i\rangle \tag{23}$$

are locally equivalent to $|\psi^{\text{GHZ-}m}\rangle$ when $\alpha_i, \beta_i \in \mathbb{R}$ for all $i$ (see Supplemental Material Appendix B [54] for the derivations).

To verify $|\psi^{\text{GHZ-}m}\rangle$, consider the following $2(m-1)$ measurement settings:

$$\Omega_{2l-1}^{\text{GHZ-}m} = \mathcal{P}_l\left\{[B_{2l-1}^{\dagger}(\mathbb{1} - \tau^- \otimes \tau^-)B_{2l-1}] \otimes \mathbb{1}^{\otimes(m-2)}\right\},$$
$$\Omega_{2l}^{\text{GHZ-}m} = \mathcal{P}_l\left\{[B_{2l}^{\dagger}(\mathbb{1} - \tau^- \otimes \tau^-)B_{2l}] \otimes \mathbb{1}^{\otimes(m-2)}\right\}, \tag{24}$$

with $l = 1, 2, \ldots, m-1$, where $B_{2l-1} = D(-\alpha_l) \otimes \mathbb{1}$ and $B_{2l} = \mathbb{1} \otimes D(-\alpha_{l+1})$ are local operations. The symbol $\mathcal{P}_l$ indicates the permutation that only the $l$ and $l+1$ modes are operated on for each setting. Moreover, we need one more measurement setting

$$\Omega_{2m-1}^{\text{GHZ-}m} = \left[\bigotimes_{i=1}^{m}D^{\dagger}\left(-\frac{\alpha_i}{2}\right)\right](\pi^{\otimes m})^+\left[\bigotimes_{i=1}^{m}D\left(-\frac{\alpha_i}{2}\right)\right], \tag{25}$$

where $(\pi^{\otimes m})^+$ is the projector onto the eigenspace with eigenvalue $+1$ of the parity measurement $\pi^{\otimes m}$. With these, we have the following theorem for verifying $|\psi^{\text{GHZ-}m}\rangle$ (see Supplemental Material Appendix F [54] for the proof).

*Theorem 2.* The $m$-mode GHZ-like coherent states $|\psi^{\text{GHZ-m}}\rangle$ can be verified efficiently by the protocol

$$\Omega^{\text{GHZ-}m} = \sum_{l=1}^{2m-1}\mu_l \Omega_l^{\text{GHZ-}m}, \tag{26}$$

where the probability distribution $\{\mu_l\}$ is arbitrary. An optimal efficiency can be obtained by optimizing $\{\mu_l\}$ under specific scenarios as constrained by Eq. (5).

Two remarks are in order. First, except for the last setting which requires PNRDs on each mode, the other $2(m-1)$ measurement settings have exactly the same framework as $\Omega^{\text{ECS}}$ shown in Fig. 1, thus only two modes are operated on each time. Second, if changing the superposition of the two terms in $|\psi^{\text{GHZ-}m}\rangle$ from $+$ to $-$, they can still be verified efficiently with similar experimental settings (see Supplemental Material Appendix G [54] for the details).

*Conclusion.* We have developed a systematic framework for verifying continuous-variable quantum states with local measurements only. Same as in the discrete-variable scenario, the high verification efficiency with the resource overhead of $N \propto O(\epsilon^{-1} \ln \delta^{-1})$ within infidelity $\epsilon$ and confidence level $1 - \delta$ is retained. This efficiency is quadratically better than quantum tomography as well as other nontomographic methods which usually require the resource in the order of $N \propto O(\epsilon^{-2} \ln \delta^{-1})$. The high verification efficiency of our protocol is confirmed with the demonstration for verifying entangled two-mode and multimode coherent states.

As an outlook, it is interesting to extend the current study to verifying other important CV quantum states, and even CV quantum processes. Also, the adversarial scenario [15,25,26,70] is worth considering, of which correlations among the input states can be included. In such a case the scaling of the verification efficiency is expected to be kept, but deteriorate by a constant factor [25,26]. Moreover, with the techniques including adaptive measurements [20,27] and nondemolition photon counting [34,71,72], our protocol has the potential for further improvement.

[1] S. L. Braunstein and P. van Loock, Quantum information with continuous variables, Rev. Mod. Phys. **77**, 513 (2005).

[2] C. Weedbrook, S. Pirandola, R. García-Patrón, N. J. Cerf, T. C. Ralph, J. H. Shapiro, and S. Lloyd, Gaussian quantum information, Rev. Mod. Phys. **84**, 621 (2012).

[3] G. M. D'Ariano, C. Macchiavello, and M. G. A. Paris, Detection of the density matrix through optical homodyne tomography without filtered back projection, Phys. Rev. A **50**, 4298 (1994).

[4] U. Leonhardt, *Measuring the Quantum State of Light* (Cambridge University Press, Cambridge, 1997), Vol. 22.

[5] G. M. D'Ariano, M. G. A. Paris, and M. F. Sacchi, Quantum tomography, Adv. Imag. Elect. Phys. **128**, 205 (2003).

[6] M. Guţă and L. Artiles, Minimax estimation of the Wigner function in quantum homodyne tomography with ideal detectors, Math. Meth. Stat. **16**, 1 (2007).

[7] S. Glancy and H. M. de Vasconcelos, Methods for producing optical coherent state superpositions, J. Opt. Soc. Am. B **25**, 712 (2008).

[8] A. I. Lvovsky and M. G. Raymer, Continuous-variable optical quantum-state tomography, Rev. Mod. Phys. **81**, 299 (2009).

[9] R. J. Donaldson, R. J. Collins, E. Eleftheriadou, S. M. Barnett, J. Jeffers, and G. S. Buller, Experimental Implementation of a Quantum Optical State Comparison Amplifier, Phys. Rev. Lett. **114**, 120505 (2015).

[10] L. Aolita, C. Gogolin, M. Kliesch, and J. Eisert, Reliable quantum certification of photonic state preparations, Nat. Commun. **6**, 8498 (2015).

[11] N. Liu, T. F. Demarie, S.-H. Tan, L. Aolita, and J. F. Fitzsimons, Client-friendly continuous-variable blind and verifiable quantum computing, Phys. Rev. A **100**, 062309 (2019).

[12] U. Chabaud, T. Douce, F. Grosshans, E. Kashefi, and D. Markham, Building trust for continuous variable quantum states, arXiv:1905.12700.

[13] U. Chabaud, F. Grosshans, E. Kashefi, and D. Markham, Efficient verification of Boson sampling, arXiv:2006.03520.

[14] U. Chabaud, G. Roeland, M. Walschaers, F. Grosshans, V. Parigi, D. Markham, and N. Treps, Certification of non-Gaussian states with operational measurements, PRX Quantum **2**, 020333 (2021).

[15] Y. Takeuchi, A. Mantri, T. Morimae, A. Mizutani, and J. F. Fitzsimons, Resource-efficient verification of quantum computing using Serflings bound, npj Quantum Inf. **5**, 27 (2019).

[16] M. Hayashi, K. Matsumoto, and Y. Tsuda, A study of LOCC-detection of a maximally entangled state using hypothesis testing, J. Phys. A: Math. Gen. **39**, 14427 (2006).

[17] S. Pallister, N. Linden, and A. Montanaro, Optimal Verification of Entangled States with Local Measurements, Phys. Rev. Lett. **120**, 170502 (2018).

[18] T. Morimae, Y. Takeuchi, and M. Hayashi, Verification of hypergraph states, Phys. Rev. A **96**, 062321 (2017).

[19] Y. Takeuchi and T. Morimae, Verification of Many-Qubit States, Phys. Rev. X **8**, 021060 (2018).

[20] X.-D. Yu, J. Shang, and O. Gühne, Optimal verification of general bipartite pure states, npj Quantum Inf. **5**, 112 (2019).

[21] Z. Li, Y.-G. Han, and H. Zhu, Efficient verification of bipartite pure states, Phys. Rev. A **100**, 032316 (2019).

[22] K. Wang and M. Hayashi, Optimal verification of two-qubit pure states, Phys. Rev. A **100**, 032315 (2019).

[23] H. Zhu and M. Hayashi, Optimal verification and fidelity estimation of maximally entangled states, Phys. Rev. A **99**, 052346 (2019).

[24] H. Zhu and M. Hayashi, Efficient Verification of Hypergraph States, Phys. Rev. Appl. **12**, 054047 (2019).

[25] H. Zhu and M. Hayashi, Efficient Verification of Pure Quantum States in the Adversarial Scenario, Phys. Rev. Lett. **123**, 260504 (2019).

[26] H. Zhu and M. Hayashi, General framework for verifying pure quantum states in the adversarial scenario, Phys. Rev. A **100**, 062335 (2019).

[27] Y.-C. Liu, X.-D. Yu, J. Shang, H. Zhu, and X. Zhang, Efficient Verification of Dicke States, Phys. Rev. Appl. **12**, 044020 (2019).

[28] Z. Li, Y.-G. Han, and H. Zhu, Optimal Verification of Greenberger-Horne-Zeilinger States, Phys. Rev. Appl. **13**, 054002 (2020).

[29] N. Dangniam, Y.-G. Han, and H. Zhu, Optimal verification of stabilizer states, Phys. Rev. Res. **2**, 043323 (2020).

[30] W.-H. Zhang, C. Zhang, Z. Chen, X.-X. Peng, X.-Y. Xu, P. Yin, S. Yu, X.-J. Ye, Y.-J. Han, J.-S. Xu, G. Chen, C.-F. Li, and G.-C. Guo, Experimental Optimal Verification of Entangled States Using Local Measurements, Phys. Rev. Lett. **125**, 030506 (2020).

[31] X. Jiang, K. Wang, K. Qian, Z. Chen, Z. Chen, L. Lu, L. Xia, F. Song, S. Zhu, and X. Ma, Towards the standardization of quantum state verification using optimal strategies, npj Quantum Inf. **6**, 90 (2020).

[32] W.-H. Zhang, X. Liu, P. Yin, X.-X. Peng, G.-C. Li, X.-Y. Xu, S. Yu, Z.-B. Hou, Y.-J. Han, J.-S. Xu, Z.-Q. Zhou, G. Chen, C.-F. Li, and G.-C. Guo, Classical communication enhanced quantum state verification, npj Quantum Inf. **6**, 103 (2020).

[33] Z. Li, Y.-G. Han, H.-F. Sun, J. Shang, and H. Zhu, Verification of phased Dicke states, Phys. Rev. A **103**, 022601 (2021).

[34] Y.-C. Liu, J. Shang, R. Han, and X. Zhang, Universally Optimal Verification of Entangled States with Nondemolition Measurements, Phys. Rev. Lett. **126**, 090504 (2021).

[35] Y.-C. Liu, J. Shang, X.-D. Yu, and X. Zhang, Efficient verification of quantum processes, Phys. Rev. A **101**, 042315 (2020).

[36] H. Zhu and H. Zhang, Efficient verification of quantum gates with local operations, Phys. Rev. A **101**, 042316 (2020).

[37] P. Zeng, Y. Zhou, and Z. Liu, Quantum gate verification and its application in property testing, Phys. Rev. Res. **2**, 023306 (2020).

[38] N. C. Menicucci, P. van Loock, M. Gu, C. Weedbrook, T. C. Ralph, and M. A. Nielsen, Universal Quantum Computation with Continuous-Variable Cluster States, Phys. Rev. Lett. **97**, 110501 (2006).

[39] F. Mattioli, Z. Zhou, A. Gaggero, R. Gaudio, R. Leoni, and A. Fiore, Photon-counting and analog operation of a 24-pixel photon number resolving detector based on superconducting nanowires, Opt. Express **24**, 9067 (2016).

[40] D. Fukuda, G. Fujii, T. Numata, K. Amemiya, A. Yoshizawa, H. Tsuchida, H. Fujino, H. Ishii, T. Itatani, S. Inoue, and T. Zama, Titanium-based transition-edge photon number resolving detector with 98% detection efficiency with index-matched small-gap fiber coupling, Opt. Express **19**, 870 (2011).

[41] A. Divochiy, F. Marsili, D. Bitauld, A. Gaggero, R. Leoni, F. Mattioli, A. Korneev, V. Seleznev, N. Kaurova, O. Minaeva, G. Gol'tsman, K. G. Lagoudakis, M. Benkhaoul, F. Lévy, and A. Fiore, Superconducting nanowire photon-number-resolving detector at telecommunication wavelengths, Nat. Photon. **2**, 302 (2008).

[42] B. E. Kardynał, Z. L. Yuan, and A. J. Shields, An avalanche-photodiode-based photon-number-resolving detector, Nat. Photon. **2**, 425 (2008).

[43] L. A. Morais, T. Weinhold, M. P. de Almeida, A. Lita, T. Gerrits, S. W. Nam, A. G. White, and G. Gillett, Precisely determining photon-number in real-time, arXiv:2012.10158.

[44] Y.-D. Wu, G. Bai, G. Chiribella, and N. Liu, Efficient Verification of Continuous-Variable Quantum States and Devices without Assuming Identical and Independent Operations, Phys. Rev. Lett. **126**, 240503 (2021).

[45] S. J. van Enk and O. Hirota, Entangled coherent states: Teleportation and decoherence, Phys. Rev. A **64**, 022313 (2001).

[46] X. Wang, Quantum teleportation of entangled coherent states, Phys. Rev. A **64**, 022302 (2001).

[47] P. T. Cochrane, G. J. Milburn, and W. J. Munro, Macroscopically distinct quantum-superposition states as a bosonic code for amplitude damping, Phys. Rev. A **59**, 2631 (1999).

[48] H. Jeong and M. S. Kim, Efficient quantum computation using coherent states, Phys. Rev. A **65**, 042305 (2002).

[49] T. C. Ralph, A. Gilchrist, G. J. Milburn, W. J. Munro, and S. Glancy, Quantum computation with optical coherent states, Phys. Rev. A **68**, 042319 (2003).

[50] A. P. Lund, T. C. Ralph, and H. L. Haselgrove, Fault-Tolerant Linear Optical Quantum Computing with Small-Amplitude Coherent States, Phys. Rev. Lett. **100**, 030503 (2008).

[51] J. Joo, W. J. Munro, and T. P. Spiller, Quantum Metrology with Entangled Coherent States, Phys. Rev. Lett. **107**, 083601 (2011).

[52] J. Joo, K. Park, H. Jeong, W. J. Munro, K. Nemoto, and T. P. Spiller, Quantum metrology for nonlinear phase shifts with entangled coherent states, Phys. Rev. A **86**, 043828 (2012).

[53] J. Liu, X.-M. Lu, Z. Sun, and X. Wang, Quantum multiparameter metrology with generalized entangled coherent state, J. Phys. A: Math. Theor. **49**, 115302 (2016).

[54] See Supplemental Material at http://link.aps.org/supplemental/10.1103/PhysRevResearch.3.L042004 for the Appendices.

[55] C. Wittmann, M. Takeoka, K. N. Cassemiro, M. Sasaki, G. Leuchs, and U. L. Andersen, Demonstration of Near-Optimal Discrimination of Optical Coherent States, Phys. Rev. Lett. **101**, 210501 (2008).

[56] M. T. DiMario and F. E. Becerra, Robust Measurement for the Discrimination of Binary Coherent States, Phys. Rev. Lett. **121**, 023603 (2018).

[57] V. Bužek, A. Vidiella-Barranco, and P. L. Knight, Superpositions of coherent states: Squeezing and dissipation, Phys. Rev. A **45**, 6570 (1992).

[58] H. Takahashi, K. Wakui, S. Suzuki, M. Takeoka, K. Hayasaka, A. Furusawa, and M. Sasaki, Generation of Large-Amplitude Coherent-State Superposition Via Ancilla-Assisted Photon Subtraction, Phys. Rev. Lett. **101**, 233605 (2008).

[59] V. V. Dodonov, I. A. Malkin, and V. I. Man'ko, Even and odd coherent states and excitations of a singular oscillator, Physica **72**, 597 (1974).

[60] A. Gilchrist, K. Nemoto, W. J. Munro, T. C. Ralph, S. Glancy, S. L. Braunstein, and G. J. Milburn, Schrödinger cats and their power for quantum information processing, J. Opt. B: Quantum Semiclass. Opt. **6**, S828 (2004).

[61] L.-M. Kuang and J.-Y. Zhu, Even and odd phase coherent states for Hermitian phase operator theory, J. Phys. A: Math. Gen. **29**, 895 (1996).

[62] J.-C. Besse, S. Gasparinetti, M. C. Collodo, T. Walter, A. Remm, J. Krause, C. Eichler, and A. Wallraff, Parity Detection of Propagating Microwave Fields, Phys. Rev. X **10**, 011046 (2020).

[63] B. C. Sanders, Entangled coherent states, Phys. Rev. A **45**, 6811 (1992).

[64] B. C. Sanders, Review of entangled coherent states, J. Phys. A: Math. Theor. **45**, 244002 (2012).

[65] W. J. Munro, G. J. Milburn, and B. C. Sanders, Entangled coherent-state qubits in an ion trap, Phys. Rev. A **62**, 052108 (2000).

[66] H. Jeong, M. S. Kim, and J. Lee, Quantum-information processing for a coherent superposition state via a mixedentangled coherent channel, Phys. Rev. A **64**, 052308 (2001).

[67] Be reminded that the noisy states in Eq. (21) are different in form from those in Eq. (4), but direct calculations can establish the relation between its passing probability and the infidelity $\epsilon$ (see Supplemental Material Appendix E [54]).

[68] Y. Israel, L. Cohen, X.-B. Song, J. Joo, H. S. Eisenberg, and Y. Silberberg, Entangled coherent states created by mixing squeezed vacuum and coherent light, Optica **6**, 753 (2019).

[69] H. Jeong and N. B. An, Greenberger-Horne-Zeilinger–type and *W*-type entangled coherent states: Generation and Bell-type inequality tests without photon counting, Phys. Rev. A **74**, 022104 (2006).

[70] M. Hayashi and T. Morimae, Verifiable Measurement-Only Blind Quantum Computing with Stabilizer Testing, Phys. Rev. Lett. **115**, 220502 (2015).

[71] W. J. Munro, K. Nemoto, R. G. Beausoleil, and T. P. Spiller, High-efficiency quantum-nondemolition single-photon-number-resolving detector, Phys. Rev. A **71**, 033819 (2005).

[72] C. Guerlin, J. Bernu, S. Deleglise, C. Sayrin, S. Gleyzes, S. Kuhr, M. Brune, J.-M. Raimond, and S. Haroche, Progressive field-state collapse and quantum non-demolition photon counting, Nature (London) **448**, 889 (2007).